ACS APPLIED MATERIALS & INTERFACES

Research Article

www.acsami.org

Hollow V_2O_5 Nanoassemblies for High-Performance Room-Temperature Hydrogen Sensors

Ying-Ting Wang, Wha-Tzong Whang, and Chun-Hua Chen*

Department of Materials Science and Engineering, National Chiao Tung University, 1001 Ta-Hsueh Road, Hsin-Chu, Taiwan 30010, ROC

Supporting Information

ABSTRACT: Nanostructured oxides with characteristic morphologies are essential building blocks for high-performance gas-sensing devices. We describe the high-yield fabrication of a series of functionalized V_2O_5 nanoassemblies through a facile polyol approach with specific varieties of polyvinylpyrrolidone. The synthesized V_2O_5 nanoassemblies consisting of tiny one-dimensional nanoblocks with the absence of any extrinsic catalysts exhibit distinct hemispherical or spherical hollow morphologies and operate as room-temperature hydrogen sensors with remarkable sensitivities and responses.

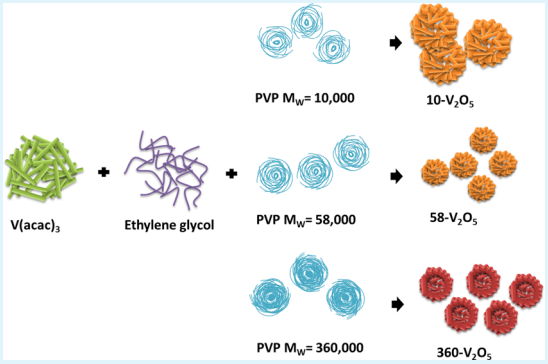

KEYWORDS: *nanoassembly, core−shell, semisphere, nanosensor*

INTRODUCTION

Explosion hazards associated with high-pressure hydrogen gas are widely regarded as one of the most important issues in developing and delivering hydrogen-based green energy systems designated for industrial and domestic purposes. The extensive concern over safety during the transport and storage of hydrogen certainly requires reliable sensors for detecting any unexpected leakage. Hydrogen gas sensors having higher performance for approaching a rapid and extremely sensitive response and lower operating temperatures for preventing explosion and saving electric power are therefore urgently required because of this extensive safety concern.[1]

Metal oxide semiconductors have been extensively investigated and recognized as the most economic materials for efficient hydrogen sensing.[2−13] However, most of these oxide sensors can be operated only at extremely high temperatures, i.e., more than several hundred degrees Celsius, because all the fundamental reactions including dissociation, adsorption, and desorption of gases on oxide surfaces are thermally activated.[14]

Lowering the operating temperature to a safer level, for instance, to room temperature, is an essential issue, but remains a challenge. A room-temperature sensor could simplify device design by eliminating the heater component, save electrical power, be assembled on flexible polymer substrates, and most importantly, avoid triggering an explosion in an explosive environment. In recent years, many researchers have made tremendous efforts toward the development of room-temperature oxide gas sensors, mainly via synthesizing unique oxide nanomaterials with very sharp one-dimensional tips[13,15,16] or decorating the oxide materials with highly active Pd or Pt nanoparticles as the catalytic reagent.[17,18] Unfortunately, the strategy using metallic catalysts appears to not work all the time.[19−23]

We focus on fabricating oxide nanostructures with highly designed structural characteristics potentially for gaining high-performance room-temperature hydrogen sensors. A hollow-core oxide nanoassembly comprising numerous nanocrystals as a shell could efficiently provide larger active surface areas and a porous configuration for enhancing the sensing reactions required and is thus specially selected as the target structure for potentially meeting the present purposes. Appropriate selection of suitable sensor materials is undoubtedly crucial for perfectly demonstrating the power of the nanostructure design. V_2O_5, a transition-metal oxide having a relatively narrow bandgap of 2.2 eV in comparison with the widely used nontransition-metal oxides such as ZnO (3.4 eV) or SnO_2 (3.7 eV)[24] was thus considered as a promising compound for the present study. Compared to the data available regarding other classes, data related to systematic synthesis of hollow V_2O_5 nanostructures and their gas-sensing applications remains lacking.[25−27]

RESULTS AND DISCUSSION

As shown in Figure 1a, the X-ray diffraction (XRD) pattern of the prepared hollow V_2O_5 nanoassemblies (10-V_2O_5) matches the recorded pattern (JCPDS entry 41-1426) well, indicating the presence only of highly crystalline orthorhombic V_2O_5 (see

Received: December 29, 2014
Accepted: April 3, 2015
Published: April 3, 2015

DOI: 10.1021/am509182s
ACS Appl. Mater. Interfaces 2015, 7, 8480−8487

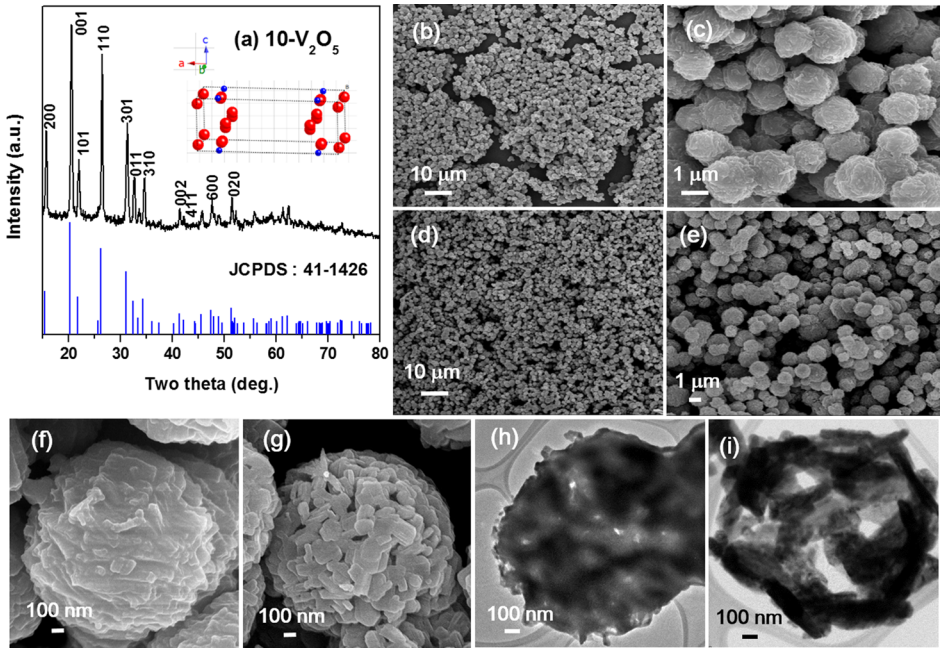

Figure 1. Orthorhombic hollow nanoassemblies of synthesized 10-V_2O_5: (a) XRD pattern, (b–g) SEM images, and (h, i) TEM images. Panels b, c, f, and h are before calcining of the 10-V_2O_5 nanoassemblies, and d, e, g, and i are after.

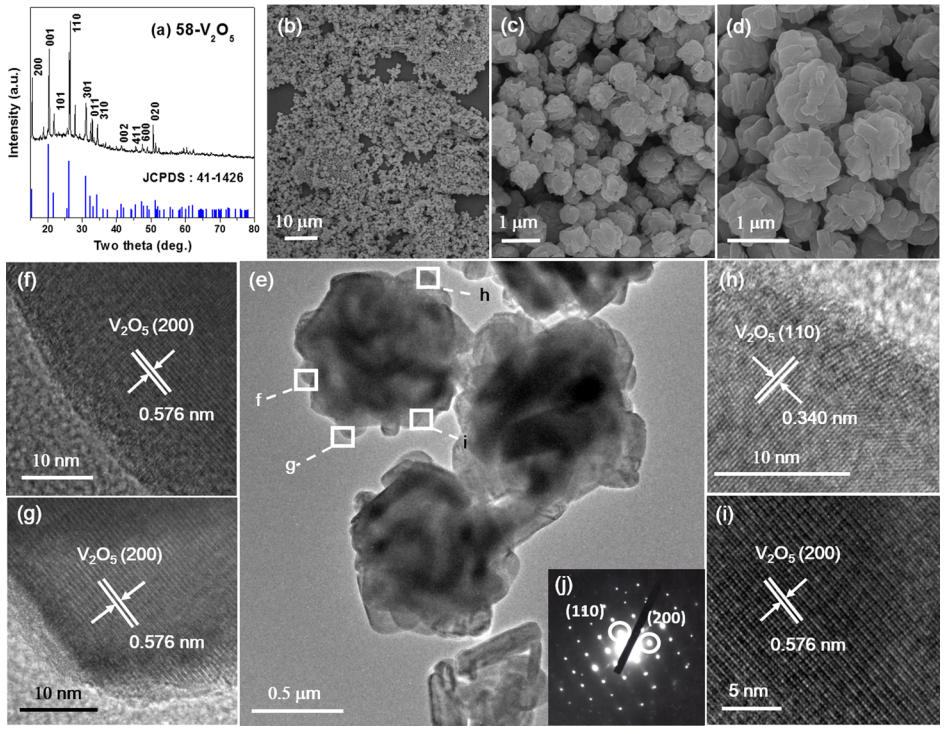

Figure 2. Orthorhombic hollow nanoassemblies of synthesized 58-V_2O_5: (a) XRD pattern and (b–d) SEM images. Panels e–i are TEM images, and panel j is the SAED pattern of region i (the tip of one branch of 58-V_2O_5).

inset) without traceable impurities. The scanning electron microscopy (SEM) observations directly confirm that the morphology and the diameter of the present nanoassemblies are rather uniform before (Figure 1b,c,f) and also after (Figure 1d,e,g) high-temperature calcination. The slight shrinkage of the spherical assemblies and the significant increase of the porosity after calcination is understandable, as can also be observed in the transmission electron microscopy (TEM) images taken from a single isolated V_2O_5 nanoassembly (Figure 1h,i). From a close look at the surface morphology (Figure 1g), it is easy to see that the randomly assembled building blocks are one-dimensional (1-D) nanorods with various diameters and lengths, which can also be confirmed in the TEM image (Figure 1i). Additionally, the image contrast of the central regions of the nanoassemblies before and after calcination is nearly as transparent as that of the edge regions, which proves that all of the V_2O_5 nanoassemblies are certainly hollow.

DOI: 10.1021/am509182s
ACS Appl. Mater. Interfaces 2015, 7, 8480–8487

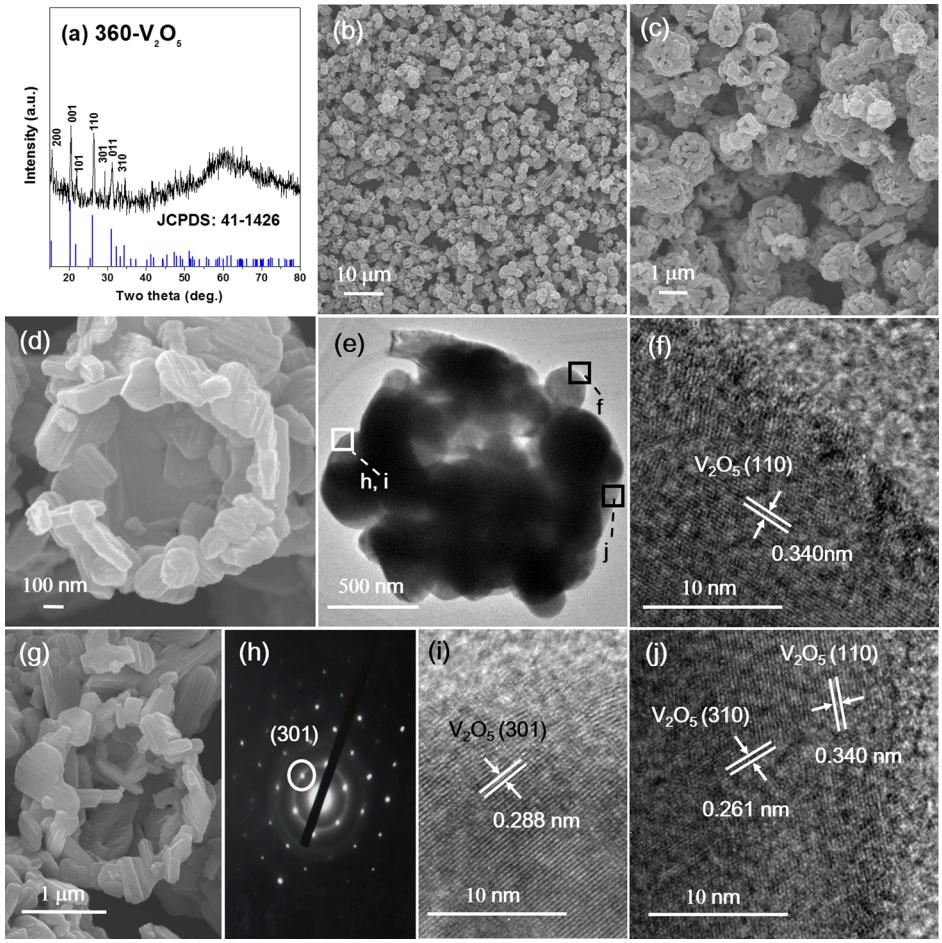

Figure 3. Orthorhombic semispherical hollow nanoassemblies of synthesized 360-V_2O_5: (a) XRD pattern and (b–d, g) SEM images. Panels e, f, i, and j are TEM images, and panel h is the SAED pattern of region i (the tip of one branch of 360-V_2O_5).

When the polyvinylpyrrolidone (PVP) of M_w = 10 000 was replaced with PVP of M_w = 58 000, the crystal structure as well as the hollow morphology of the prepared V_2O_5 nanoassemblies (denoted as 58-V_2O_5) is rather similar to that of 10-V_2O_5, as evidenced in Figure 2a and Figure 2b–d, respectively. The TEM image shown in Figure 2e evidently proves that the V_2O_5 nanoassemblies are hollow like other specimens. To clarify the crystallinity of the 1-D building block of the nanoassemblies, the high-resolution TEM images (HRTEM) taken from four tips around one V_2O_5 nanoassembly as marked with squares (Figure 2f–i) confirm that the nanorods are all single crystalline, as also evidenced by the selected area electron diffraction (SAED) pattern of region i.

When the molecular weight of PVP further increases to M_w = 360 000, basically the crystal structure and the uniform spherical morphology of the V_2O_5 nanoassembly (denoted as 360-V_2O_5) were maintained, as can be confirmed by the XRD pattern (Figure 3a) and the SEM (Figure 3b–f) or TEM (Figure 3g) images, respectively. However, as clearly observed in the SEM images, the shells of these V_2O_5 nanoassemblies are semispherical and in general more porous than those of 10-V_2O_5 and 58-V_2O_5. The close-up SEM images of the semispherical hollow 360-V_2O_5 provide an inner view of the hollow nanoassemblies, which evidently indicate that a uniform shell could be formed. The HRTEM images (Figure 3f,i,j) and the SAED pattern of region i as marked in Figure 3e confirm that the nanorods are all single crystalline, as in 10-V_2O_5 and 58-V_2O_5. It is worth emphasizing that the significant change of the assembling morphology from hollow spheres to semispheres by simply adjusting the molecular weight of PVP is a great breakthrough.

It has been found that PVP would act as not only a surfactant but also a soft template in the ethylene glycol (EG ($C_2H_6O_2$)) solution.[28,29] When V(acac)$_3$ (VO($C_5H_7O_2$)$_2$) was dissolved in EG, the acac ligands would be gradually replaced with EG to form vanadium glycolates (VO(OCH_2–CH_2O)). The oligomerization processes would then lead to the growth of tiny VO(OCH_2–CH_2O) nanorods. In the present synthesis, PVP comprising hydrophobic vinyl groups and hydrophilic carbonyl groups would form hydrophilic spherical micelles in EG. The VO(OCH_2–CH_2O) nanorods would thus spontaneously assemble on the spherical PVP template via hydrogen bonds to have a hollow structure.

According to the above results, the molecular weight of PVP induces significant changes not only in the morphology but also in the size of the formed V_2O_5 nanoassemblies. In the group of the spherical hollow V_2O_5 nanoassemblies, a lower molecular weight of PVP leads to a larger diameter, where the size of 10-V_2O_5 and 58-V_2O_5 is around 1.0–1.5 and 0.6–1.0 μm, respectively (Figures 1 and 2). A much higher PVP molecular weight (360-V_2O_5) interestingly leads to a semispherical hollow with a diameter of around 2.0 μm.

The surface tension of homologous series of polymers tends to increase with molecular weight:[30]

DOI: 10.1021/am509182s
ACS Appl. Mater. Interfaces 2015, 7, 8480–8487

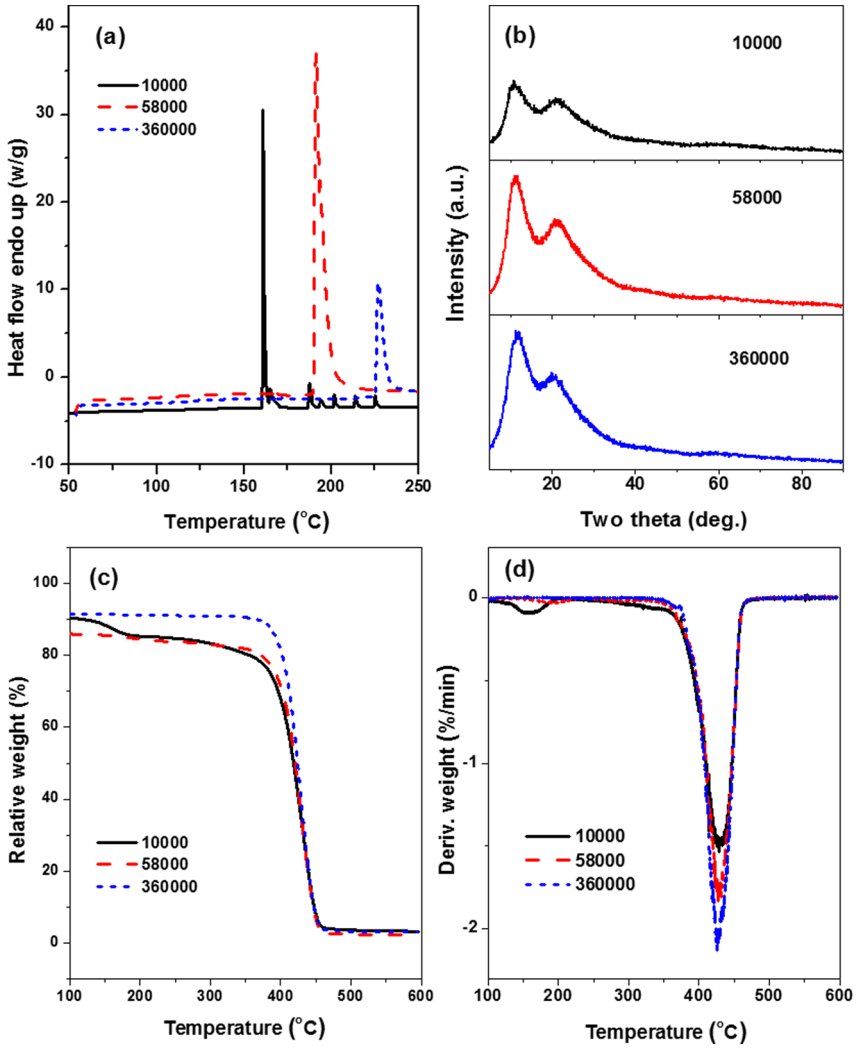

Figure 4. (a) DSC, (b) XRD, (c) thermogravimetric analyses (TGA) using a temperature ramp of 2 °C/min, and (d) derivative of the TGA curves of PVP with a molecular weight of 10 000, 58 000, and 360 000.

$$\gamma = \gamma_{\infty} - K_e/M_w^{2/3} \quad (1)$$

$$K_e \approx (\gamma_{\infty} - \gamma_e)(2m)^{2/3} \quad (2)$$

where γ is the surface tension, γ_{∞} the surface tension at infinite molecular weight, M_w the molecular weight, K_e a constant, γ_e the surface tension of the end groups, and m the formula weight of the repeat units.

In addition, the effect of surface tension on curvature can be expressed as

$$\gamma/\gamma_0 = (1 + 2t/R)^{-1} \quad (3)$$

where γ_0 is the surface tension across a flat interface, t the surface layer thickness on the order of 10^{-8} cm, and R the drop radius.

According to the above equations, the increase of the molecular weight of PVP from M_w = 10 000 to M_w = 58 000 would lead to the decrease of the drop radius of PVP and thus the size reduction of the spherical V_2O_5 nanoassemblies.

From the analyses of differential scanning calorimetry (DSC) (Figure 4a), sharp endothermic peaks at 160.83, 191.33, and 226.95 °C are found for PVP of M_w = 10 000, M_w = 58 000, and M_w = 360 000, respectively, indicating the molecular weight dependence of the melting point. The XRD patterns (Figure 4b) confirm that a higher molecular weight leads to a smaller full width at half-maximum (fwhm), that is, a larger crystalline size, which is in agreement with the DSC result.

Because the V_2O_5 nanoassemblies were fabricated with high-temperature calcination at around 200−250 °C, the PVP should be in a liquid state for M_w = 10 000 and M_w = 58 000 but in a rubbery state for M_w = 360 000. Moreover, accompanying the faster decomposition rate of PVP of M_w = 360 000 (Figure 4c,d), it is reasonably to consider that the semispherical hollow morphology (360-V_2O_5) originated from the violent disintegration of a relatively hard spherical template. In contrast, the slower decomposition rate for M_w = 10 000 and M_w = 58 000 under a liquid state certainly maintains the complete spherical morphology.

The scanning electron microscopy energy-dispersive spectrometry (SEM-EDS) elemental analyses confirm the non-stoichiometry of the prepared hollow V_2O_5 nanoassemblies (see Table S1 in Supporting Information). In general, insufficiency of oxygen is frequently observed in oxides, which will create oxygen vacancies in the oxides and the consequent unique photoluminescence (PL) properties. However, in contrast to 10-V_2O_5 and 58-V_2O_5, an unusually large deviation from the stoichiometric ratio was found for 360-

DOI: 10.1021/am509182s
ACS Appl. Mater. Interfaces 2015, 7, 8480−8487

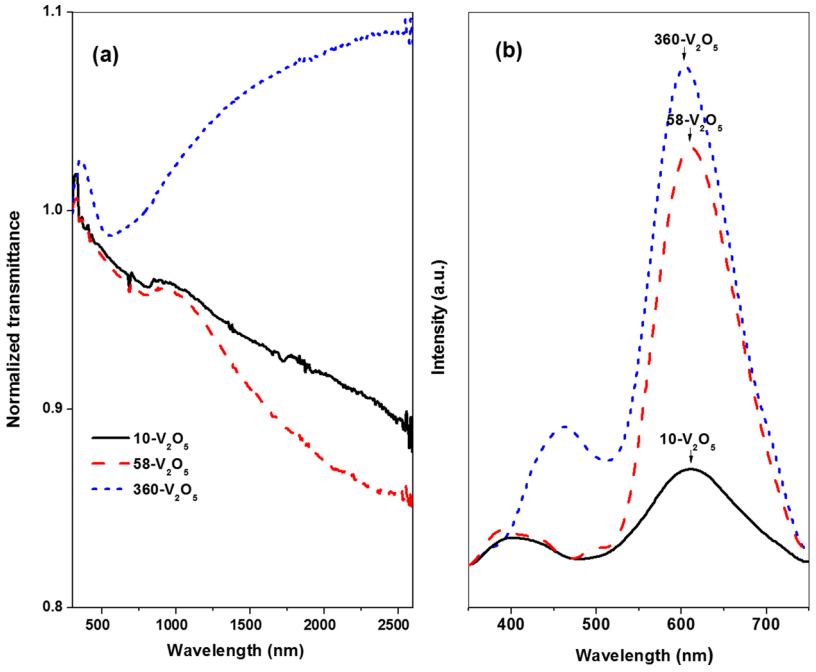

Figure 5. (a) Normalized UV−vis−NIR transmittance spectra and (b) PL spectra of 10-V_2O_5, 58-V_2O_5, and 360-V_2O_5.

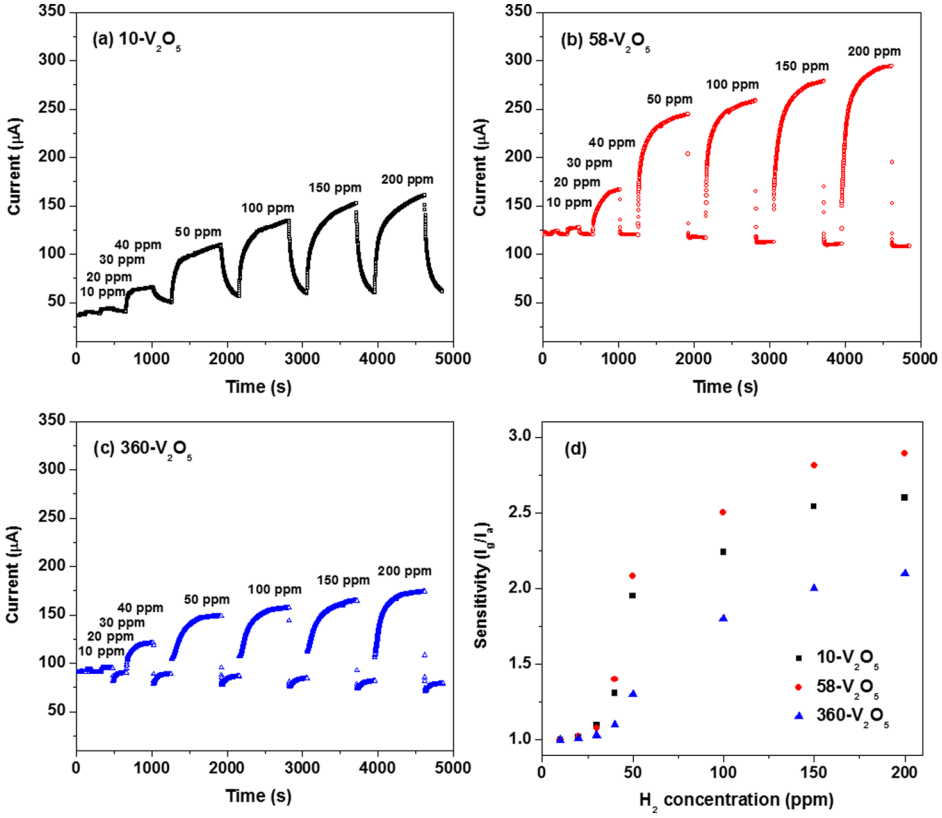

Figure 6. Room-temperature dynamic response and recovery curves for (a) 10-V_2O_5, (b) 58-V_2O_5, and (c) 360-V_2O_5 under 10−200 ppm of H_2 and (d) the corresponding sensitivities (I_g/I_a).

V_2O_5, which evidently originates from the slight presence of VO_2 in 360-V_2O_5, as quantitatively identified by X-ray photoelectron microscopy (XPS; Figure S1 in Supporting Information). In addition, the well-fitted XPS profiles (Figure S1a,b in Supporting Information) suggest that the present synthesis overcomes the difficulty in preparing highly pure V_2O_5.[31−34]

Figure 5 shows the ultraviolet−visible−near-infrared (UV−vis−NIR) and PL spectra of 10-V_2O_5, 58-V_2O_5, and 360-V_2O_5. To compare the characteristic features of these three structures, the transmittance spectra obtained were normalized. Surpris-

DOI: 10.1021/am509182s
ACS Appl. Mater. Interfaces 2015, 7, 8480−8487

ingly, relatively high transmittance from the visible to the near-IR region was observed only for 360-V_2O_5. According to several independent studies regarding the nanostructures with cup- or bowl-like morphologies,[35−37] the very special semispherical shell morphology shown in 360-V_2O_5 would likely lead to rising trends of the transmittance from the visible to the near-IR region. In addition, the existence of VO_2 in 360-V_2O_5 (as discussed in Figure S1 in Supporting Information) might also slightly contribute to the higher transmittance from the visible to the near-IR region as previously reported.[38] The significant difference in the UV−vis−NIR spectra certainly provides unique options in a variety of potential applications. Similar to Figure 5a, the PL spectra shown in Figure 5b also reflect the morphological difference between the spherical (10-V_2O_5 and 58-V_2O_5) and semispherical (360-V_2O_5) hollow structures. The main PL peaks found around 604−612 nm for these three hollow V_2O_5 nanoassemblies correspond to the bandgap of V_2O_5 (~2 eV). The minor PL peak around 450 nm clearly displayed in 360-V_2O_5 confirms the existence of VO_2.[39,40]

Figure 6a−c shows the room-temperature sensing cycles of the three types of hollow V_2O_5 nanoassemblies prepared under various H_2 concentrations (from 10 to 200 ppm). The very sharp response and recovery curves are direct evidence that these three V_2O_5 nanoassemblies are promising materials for effectively sensing H_2 gas at room temperature. The response/recovery times obtained are 30/5 s, 40/40 s, and 50/10 s for 58-V_2O_5, 10-V_2O_5, and 360-V_2O_5, respectively, which are considered to be remarkably high response and recovery speeds for any kind of semiconducting oxide sensors at such relatively low temperatures and H_2 concentrations. For most of the oxide materials, decoration of metallic catalysts is generally required for operating at room temperature.[17,18] It is worth emphasizing that the present hollow V_2O_5 nanoassemblies evidently sense H_2 gas at room temperature without loading any extrinsic catalysts. We believe that the sharp corners or edges of the tiny building blocks for the present hollow V_2O_5 nanoassemblies (see SEM or TEM images) might be considered as highly active zones for promoting the catalytic reactions required in sensing hydrogen gas at room temperature.

The obtained sensitivities for each type of hollow V_2O_5 nanoassemblies as summarized in Figure 6d are functions of the hydrogen concentration. The sensitivity is defined as the ratio of the stabilized electric current in hydrogen (I_g) to that in air (I_a). To our knowledge, the present records are remarkably higher than those previously reported under the same sensing conditions.[41−44] It is reasonable to believe that the key factor for the present excellent results is strongly related to the hollow and porous morphology of the nanoassemblies which provide the required accessible large surface areas for sensing reactions. The measured specific surface areas (Brunauer−Emmett−Teller (BET) method) are 356, 235, and 167 $m^2 g^{-1}$ for 58-V_2O_5, 10-V_2O_5, and 360-V_2O_5, respectively, which is in good agreement with the ranking of the sensitivity of these three V_2O_5 nanoassemblies. It has been extensively observed that nanoassemblies with higher surface-to-volume ratios generally exhibit higher sensitivities and shorter response/recovery times.[15,45−47] The smaller building blocks of the sensing materials might easily lead to significant changes of the volume ratio of the depletion regions and thus the high sensitivity during the switching between the absorbing and desorbing state of the target molecules. From the present result, it is thus worth emphasizing that the concept in fabricating extremely porous nanoassemblies, such as hollow or semihollow shells, as high-performance gas sensors has been well demonstrated. With the similar concept, Hassan et al. have also demonstrated another class of excellent room-temperature hydrogen sensors comprising ZnO nanorods arrays grown on *c*-plane sapphire substrate with the absence of decoration of tiny metallic catalysts.[13] Obviously, the highly porous frameworks play a very crucial role in these successful cases.

CONCLUSIONS

Hollow V_2O_5 nanoassemblies have been successfully prepared with the goals of decreasing the working temperature to room temperature and enhancing performance in H_2 sensing. The innovative sensing platforms demonstrated excellent response and recovery speeds as well as stable H_2 concentration-dependent sensitivities at a very low operating temperature of 25 °C. The distinct architectures of the V_2O_5 nanoassemblies, with extreme porosity in the stacking configuration, play a key role in these unusual findings without any tiny catalytic metal nanoparticles. The present result evidently proves that the structural strategies applied could be one of the most promising guides for developing advanced oxide-based gas sensors.

EXPERIMENTAL SECTION

Samples of 0.25 g of $V(acac)_3$ and 0.5 g of polyvinylpyrrolidone (PVP, M_w = 10 000, 58 000, and 360 000) were dissolved in 50 mL of ethylene glycol. The dark mixture was then heated to 140 °C under stable stirring for 40 min. The formed precipitation was collected by centrifugation and then repeatedly washed with alcohol to remove residual chemicals. After drying at 60 °C in air, the powders were annealed at 500 °C in air for 2 h to form the hollow V_2O_5 nanoassemblies. The synthesized products were characterized with an X-ray diffractometer (XRD, Bruker D2), a field-emission scanning electron microscope (FE-SEM, JSM-6500), and a field-emission transmission electron microscope (FE-TEM, JEOL JEM-2100F). For FE-TEM observation, trace amounts of the prepared specimens were removed from the substrates and then suspended in ethanol solution by ultrasonication. A drop of this suspension was placed onto a copper microgrid coated with an amorphous carbon film, followed by a drying process at 60 °C for 24 h in air. The transmission spectra were determined by a UV−vis−NIR spectrophotometer (JASCO V-630). The oxidation of each component in V_2O_5 was characterized by X-ray photoelectron microscopy (Thermo VG350). All the recorded spectra were corrected by external Pt signals to prevent the charge effect. V_2O_5 were measured in the wavelength range of 350−750 nm using a self-assembly photoluminescence apparatus equipped with a 325 nm He−Cd laser (HORIBA Jobin Yvon iHR-320). Two Au electrodes aligned parallel to each other with an interspace of 1 mm are thermally deposited on a SiO_2 insulated silicon substrate. A suspension of the synthesized V_2O_5 was then dropped onto the electrode patterned substrate and then dried at 60 °C for 24 h. The dried gas sensor was preconditioned for 1 h at the measurement temperature under flowing dry air before each set of sensing measurements. The H_2 gas sensing evaluation was performed by allowing the dry air and the forming gas (H_2:N_2 = 3:97 in volume ratio) into the chamber in alternative manner, and the H_2 content was adjusted by modulating the inlet flow rate of the forming gas. During the examination, the substrate temperature was 25 °C, external bias was 1.0 V supplied by a Keithley 2400 *I*−*V* source-meter, and the electrical performance of the sensor was recorded in situ by a PC-based data acquisition system.

ASSOCIATED CONTENT

Supporting Information

SEM-EDS analyses and XPS spectra. This material is available free of charge via the Internet at http://pubs.acs.org.

DOI: 10.1021/am509182s
ACS Appl. Mater. Interfaces 2015, 7, 8480−8487

AUTHOR INFORMATION

Corresponding Author

*E-mail: ChunHuaChen@mail.nctu.edu.tw. Tel: +886-3-5131287. Fax: +886-3-5724727.

Notes

The authors declare no competing financial interest.

REFERENCES

(1) Liu, P.; Lee, S. H.; Cheong, H. M.; Tracy, C. E.; Pitts, J. R.; Smith, R. D.; Liu, P.; Lee, S. H.; Cheong, H. M.; Tracy, C. E.; Pitts, J. R.; Smith, R. D. Stable Pd/V_2O_5 Optical H_2 Sensor. *J. Electrochem. Soc.* **2002**, *149*, H76−H80.

(2) Wang, B.; Zhu, L. F.; Yang, Y. H.; Xu, N. S.; Yang, G. W. Fabrication of a SnO_2 Nanowire Gas Sensor and Sensor Performance for Hydrogen. *J. Phys. Chem. C* **2008**, *112*, 6643−6647.

(3) Myung, S.; Heo, K.; Lee, M.; Choi, Y. H.; Hong, S. H.; Hong, S. 'Focused' Assembly of V_2O_5 Nanowire Masks for the Fabrication of Metallic Nanowire Sensors. *Nanotechnology* **2007**, *18*, 205304.

(4) Shen, Y.; Yamazaki, T.; Liu, Z. F.; Meng, D.; Kikuta, T. Hydrogen Sensors Made of Undoped and Pt-Doped SnO_2 Nanowires. *J. Alloys Compd.* **2009**, *488*, L21−L25.

(5) Qurashi, A.; Tabet, N.; Faiz, M.; Yamzaki, T. Ultra-Fast Microwave Synthesis of ZnO Nanowires and Their Dynamic Response toward Hydrogen Gas. *Nanoscale Res. Lett.* **2009**, *4*, 948−954.

(6) Khan, R.; Ra, H. W.; Kim, J. T.; Jang, W. S.; Sharma, D.; Im, Y. H. Ethylene Glycol-Mediated Synthesis of Metal Oxide Nanowires. *Sens. Actuators, B* **2010**, *150*, 389−393.

(7) Imawan, C.; Steffes, H.; Solzbacher, F.; Obermeier, E. Structural and Gas-Sensing Properties of V_2O_5-MoO_3 Thin Films for H_2 Detection. *Sens. Actuators, B* **2001**, *77*, 346−351.

(8) Huh, J.; Park, J.; Kim, G. T.; Park, J. Y. Highly Sensitive Hydrogen Detection of Catalyst-Free ZnO Nanorod Networks Suspended by Lithography-Assisted Growth. *Nanotechnology* **2011**, *22*, 085502.

(9) Qurashi, A.; Yamazaki, T.; El-Maghraby, E. M.; Kikuta, T. Fabrication and Gas Sensing Properties of In_2O_3 Nanopushpins. *Appl. Phys. Lett.* **2009**, *95*, 153109.

(10) Qurashi, A.; El-Maghraby, E. M.; Yamazaki, T.; Shen, Y.; Kikuta, T. A Generic Approach for Controlled Synthesis of In_2O_3 Nanostructures for Gas Sensing Applications. *J. Alloys Compd.* **2009**, *481*, L35−L39.

(11) Qurashi, A.; El-Maghraby, E. M.; Yamazaki, T.; Kikuta, T. Catalyst Supported Growth of In_2O_3 Nanostructures and Their Hydrogen Gas Sensing Properties. *Sens. Actuators, B* **2010**, *147*, 48−54.

(12) Hoa, N. D.; Quy, N. V.; Tuan, M. A.; Hieu, N. V. Facile Synthesis of P-type Semiconducting Cupric Oxide Nanowires and Their Gas-Sensing Properties. *Phys. E (Amsterdam, Neth.)* **2009**, *42*, 146−149.

(13) Hassan, J. J.; Mahdi, M. A.; Chin, C. W.; Abu-Hassan, H.; Hassan, Z. A High-Sensitivity Room-Temperature Hydrogen Gas Sensor Based on Oblique and Vertical ZnO Nanorod Arrays. *Sens. Actuators, B* **2013**, *176*, 360−367.

(14) Choi, K. J.; Jang, H. W. One-Dimensional Oxide Nanostructures as Gas-Sensing Materials: Review and Issues. *Sensors* **2010**, *10*, 4083−4099.

(15) Agarwala, S.; Lim, Z. H.; Nicholson, E.; Ho, G. W. Probing the Morphology-Device Relation of Fe_2O_3 Nanostructures towards Photovoltaic and Sensing Applications. *Nanoscale* **2012**, *4*, 194−205.

(16) Lim, Z. H.; Chia, Z. X.; Kevin, M.; Wong, A. S. W.; Ho, G. W. A facile Approach towards ZnO Nanorods Conductive Textile for Room Temperature Multifunctional Sensors. *Sens. Actuators, B* **2010**, *151*, 121−126.

(17) Lee, J. M.; Park, J. E.; Kim, S.; Kim, S.; Lee, E.; Kim, S. J.; Lee, W. Ultra-Sensitive Hydrogen Gas Sensors Based on Pd-Decorated Tin Dioxide Nanostructures: Room Temperature Operating Sensors. *Int. J. Hydrogen Energy* **2010**, *35*, 12568−12573.

(18) Lai, H. Y.; Chen, C. H. Highly Sensitive Room-Temperature CO Gas Sensors: Pt and Pd Nanoparticle-Decorated In_2O_3 Flower-like Nanobundles. *J. Mater. Chem.* **2012**, *22*, 13204−13208.

(19) Xiang, Q.; Meng, G. F.; Zhang, Y.; Xu, J. Q.; Xu, P. C.; Pan, Q. Y.; Yu, W. J. Ag Nanoparticle Embedded-ZnO Nanorods Synthesized via a Photochemical Method and its Gas-Sensing Properties. *Sens. Actuators, B* **2010**, *143*, 635−640.

(20) Liu, X. H.; Zhang, J.; Guo, X. Z.; Wu, S. H.; Wang, S. R. Amino Acid-Assisted One-Pot Assembly of Au, Pt Nanoparticles onto One-Dimensional ZnO Microrods. *Nanoscale* **2010**, *2*, 1178−1184.

(21) Lin, Y. H.; Hsueh, Y. C.; Lee, P. S.; Wang, C. C.; Wu, J. M.; Perng, T. P.; Shih, H. C. Fabrication of Tin Dioxide Nanowires with Ultrahigh Gas Sensitivity by Atomic Layer Deposition of Platinum. *J. Mater. Chem.* **2011**, *21*, 10552−10558.

(22) Xue, X. Y.; Chen, Z. H.; Ma, C. H.; Xing, L. L.; Chen, Y. J.; Wang, Y. G.; Wang, T. H. One-Step Synthesis and Gas-Sensing Characteristics of Uniformly Loaded Pt@SnO_2 Nanorods. *J. Phys. Chem. C* **2010**, *114*, 3968−3972.

(23) Kim, S. J.; Hwang, I. S.; Na, C. W.; Kim, I. D.; Kang, Y. C.; Lee, J. H. Ultrasensitive and Selective C_2H_5OH Sensors using Rh-Loaded In_2O_3 Hollow Spheres. *J. Mater. Chem.* **2011**, *21*, 18560−18567.

(24) Wang, C. X.; Yin, L. W.; Zhang, L. Y.; Xiang, D.; Gao, R. Metal Oxide Gas Sensors: Sensitivity and Influencing Factors. *Sensors* **2010**, *10*, 2088−2106.

(25) Sasidharan, M.; Nanda, G.; Masaki, Y.; Kenichi, N. V_2O_5 Hollow Nanospheres: A Lithium Intercalation Host with Good Rate Capability and Capacity Retention. *J. Electrochem. Soc.* **2012**, *159*, A618−A621.

(26) Su, D. W.; Dou, S. X.; Wang, G. X. Hierarchical Orthorhombic V_2O_5 Hollow Nanospheres as High Performance Cathode Materials for Sodium-Ion Batteries. *J. Mater. Chem. A* **2014**, *2*, 11185−11194.

(27) Yang, J.; Lan, T.; Liu, J.; Song, Y.; Wei, M. Supercapacitor Electrode of Hollow Spherical V_2O_5 with a High Pseudocapacitance in Aqueous Solution. *Electrochim. Acta* **2013**, *105*, 489−495.

(28) Jiang, X. C.; Wang, Y. L.; Herricks, T.; Xia, Y. N. Ethylene Glycol-Mediated Synthesis of Metal Oxide Nanowires. *J. Mater. Chem.* **2004**, *14*, 695−703.

(29) Park, J. H.; Oh, C.; Shin, S. I.; Moon, S. K.; Oh, S. G. Preparation of Hollow Silica Microspheres in W/O Emulsions with Polymers. *J. Colloid Interface Sci.* **2003**, *266*, 107−114.

(30) Wu, S. *Polymer Interface and Adhesion*; Marcel Dekker, Inc: New York, 1982; pp 8, 72.

(31) Pinna, N.; Wild, U.; Urban, J.; Schlogl, R. Divanadium Pentoxide Nanorods. *Adv. Mater. (Weinheim, Ger.)* **2003**, *15*, 329−331.

(32) Xiong, C. R.; Aliev, A. E.; Gnade, B.; Balkus, K. J. Fabrication of Silver Vanadium Oxide and V_2O_5 Nanowires for Electrochromics. *ACS Nano* **2008**, *2*, 293−301.

(33) Olivetti, E. A.; Kim, J. H.; Sadoway, D. R.; Asatekin, A.; Mayes, A. M. Sol-gel Synthesis of Vanadium Oxide within A Block Copolymer Matrix. *Chem. Mater.* **2006**, *18*, 2828−2833.

(34) Sathiya, M.; Prakash, A. S.; Ramesha, K.; Tarascon, J. M.; Shukla, A. K. V_2O_5-Anchored Carbon Nanotubes for Enhanced Electrochemical Energy Storage. *J. Am. Chem. Soc.* **2011**, *133*, 16291−16299.

(35) Lu, J.; Zhang, P.; Li, A.; Su, F.; Wang, T.; Liu, Y.; Gong, J. Mesoporous Anatase TiO_2 Nanocups with Plasmonic Metal Decoration for Highly Active Visible-Light Photocatalysis. *Chem. Commun. (Cambridge, U.K.)* **2013**, *49*, 5817−5819.

(36) Mishra, Y. K.; Adelung, R.; Kumar, G.; Elbahri, M.; Mohapatra, S.; Singhal, R.; Tripathi, A.; Avasthi, D. K. Formation of Self-Organized Silver Nanocup-Type Structures and their Plasmonic Absorption. *Plasmonics* **2013**, *8*, 811−815.

(37) Butet, J.; Russier-Antoine, I.; Jonin, C.; Lascoux, N.; Benichou, E.; Brevet, P. F. Effect of the Dielectric Core and Embedding Medium on the Second Harmonic Generation from Plasmonic Nanoshells: Tunability and Sensing. *J. Phys. Chem. C* **2013**, *117*, 1172−1177.

(38) Wang, Y. T.; Chen, C. H. Facile Growth of Thermochromic VO_2 Nanostructures with Greatly Varied Phases and Morphologies. *Inorg. Chem.* **2013**, *52*, 2550−2555.

DOI: 10.1021/am509182s
ACS Appl. Mater. Interfaces 2015, 7, 8480−8487

(39) Srivastava, A.; Herng, T. S.; Saha, S.; Nina, B.; Annadi, A.; Naomi, N.; Liu, Z. Q.; Dhar, S.; Ariando; Ding, J.; Venkatesan, T. Coherently Coupled ZnO and VO_2 Interface Studied by Photoluminescence and Electrical Transport across a Phase Transition. *Appl. Phys. Lett.* **2012**, *100*, 241907.
(40) Chen, C.; Fan, Z. Changes in VO_2 Band Structure Induced by Charge Localization and Surface Segregation. *Appl. Phys. Lett.* **2009**, *95*, 262106.
(41) Lupan, O.; Chai, G.; Chow, L. Fabrication of ZnO Nanorod-Based Hydrogen Gas Nanosensor. *Microelectron. J.* **2007**, *38*, 1211−1216.
(42) Lupan, O.; Chai, G.; Chow, L. Novel Hydrogen Gas Sensor Based on Single ZnO Nanorod. *Microelectron. Eng.* **2008**, *85*, 2220−2225.
(43) Lupan, O.; Emelchenko, G. A.; Ursaki, V. V.; Chai, G.; Redkin, A. N.; Gruzintsev, A. N.; Tiginyanu, I. M.; Chow, L.; Ono, L. K.; Cuenya, B. R.; Heinrich, H.; Yakimov, E. E. Synthesis and Characterization of ZnO Nanowires for Nanosensor Applications. *Mater. Res. Bull.* **2010**, *45*, 1026−1032.
(44) Lupan, O.; Ursaki, V. V.; Chai, G.; Chow, L.; Emelchenko, G. A.; Tiginyanu, I. M.; Gruzintsev, A. N.; Redkin, A. N. Selective Hydrogen Gas Nanosensor Using Individual ZnO Nanowire with Fast Response at Room Temperature. *Sens. Actuators, B* **2010**, *144*, 56−66.
(45) Lu, F.; Liu, Y.; Dong, M.; Wang, X. P. Nanosized Tin Oxide as the Novel Material with Simultaneous Detection Towards CO, H_2 and CH_4. *Sens. Actuators, B* **2000**, *66*, 225−227.
(46) Volanti, D. P.; Felix, A. A.; Orlandi, M. O.; Whitfield, G.; Yang, D.-J.; Longo, E.; Tuller, H. L.; Varela, J. A. The Role of Hierarchical Morphologies in the Superior Gas Sensing Performance of CuO-Based Chemiresistors. *Adv. Funct. Mater.* **2013**, *23*, 1759−1766.
(47) Xi, G. C.; Ye, J. H. Ultrathin SnO_2 Nanorods: Template- and Surfactant-Free Solution Phase Synthesis, Growth Mechanism, Optical, Gas-Sensing, and Surface Adsorption Properties. *Inorg. Chem.* **2010**, *49*, 2302−2309.

DOI: 10.1021/am509182s
ACS Appl. Mater. Interfaces 2015, 7, 8480−8487